

# Direct observation of phase transformation anisotropy in indented silicon studied by confocal Raman spectroscopy

Yvonne B. Gerbig,<sup>1</sup> Stephan J. Stranick,<sup>2</sup> and Robert F. Cook<sup>1,\*</sup>

<sup>1</sup>*Ceramics Division, National Institute of Standards and Technology, Gaithersburg, Maryland 20899, USA*

<sup>2</sup>*Surface and Microanalysis Science Division, National Institute of Standards and Technology, Gaithersburg, Maryland 20899, USA*

(Received 26 January 2011; published 31 May 2011)

The theoretically predicted anisotropic nature of the indentation phase transformation in silicon (Si) is observed directly in experiments using hyperspectral, confocal Raman microscopy. The anisotropy is reflected in the two-dimensional distribution of the residual diamond cubic Si-I phase and high-pressure phases in indented Si(001), Si(110), and Si(111) surfaces, and is linked to the number and orientation of the  $\{111\}$ (110) slip systems of the diamond cubic phase that are activated during indentation. Key to the observation of the anisotropic phase transformation is the local preservation of Si-I in the residual contact impression, which is controlled by the magnitude of the applied indentation strain,  $\varepsilon_1$ . The condition for islands of Si-I to be retained after indentation is  $0.04 < \varepsilon_1 < 0.01$ ; strains outside of this range either do not result in a residual contact impression or completely transform the contacted material, rendering the underlying anisotropy of the phase transformation unobservable.

DOI: [10.1103/PhysRevB.83.205209](https://doi.org/10.1103/PhysRevB.83.205209)

PACS number(s): 78.30.Am, 61.50.Ks, 78.55.Ap, 81.70.Bt

## I. INTRODUCTION

Knowledge regarding the transformations between the various phases of silicon (Si) is critical to the design, production, and operation of Si-based structures.<sup>1-3</sup> For example, the transformation from diamond cubic Si-I to the tetragonal  $\beta$ -tin Si-II structure under mechanical loading causes changes in the electrical properties from semiconducting to metallic,<sup>4</sup> and in the mechanical behavior from brittle to ductile.<sup>5</sup> As a consequence, the mechanically induced phase transformation of Si, as in indentation experiments, is one of the most studied solid-solid phase transformations in condensed matter.<sup>6</sup> However, to date, experimental studies have only just begun to reveal the complex nature of these phase transformations in the localized zone of material adjacent to indentation sites. By analyzing cross sections cut perpendicular to indented Si surfaces, transmission electron microscopy studies have shown the presence of an inhomogeneous distribution of metastable high-pressure phases within the transformation zone.<sup>7-9</sup> Due to the dependence of the phase transformation on the magnitudes of the hydrostatic pressure and deviatoric stress, this inhomogeneity is thought to be caused by variations in the stress field induced by the indenter. Given the lack of experimental detail to the contrary, most attempts to link the stress field to the phase distribution in Si employ a simplified model of isotropic deformation<sup>8-10</sup> that disregards the effects that the anisotropic crystal structure of Si may have on the distribution of stress and ultimately on the induced phases. The influence of the crystallographic structure of Si on its phase transformation has been emphasized in theoretical studies that predict the accumulation of high-pressure phases<sup>11-13</sup> along active slip directions.<sup>12,13</sup> However, to date these predictions have not been validated experimentally. In this work, the distributions of metastable phases in indented Si were mapped in planes parallel to indented surfaces in a nondestructive manner by hyperspectral, confocal Raman microscopy (CRM). This approach and the selected experimental parameters enabled the direct observation of the inhomogeneous and anisotropic phase transformation of indented Si and the influence of crystallographic orientation on the resulting phase distribution.

The results here extend previous observations of indented Si, in which CRM was used to map the anisotropic distributions of stress exterior to the residual contact impression,<sup>14,15</sup> to the use of CRM in the identification and distributions of phase transformations within the contact impression.

## II. EXPERIMENTAL DETAILS

The test samples and indentation and CRM measurement procedures were the same as those used in a prior study.<sup>14</sup> Briefly, Si(001), Si(110), and Si(111) disks were indented at room temperature in a nitrogen-rich atmosphere with a conospherical diamond tip of nominal radius  $5 \mu\text{m}$  to a peak load of 80 mN using  $5 \text{ mN s}^{-1}$  loading and unloading rates. A conospherical rather than a pyramidal indenter was used such that the indentation deformation field was determined by the symmetry of the crystal structure of the test samples. The Si(001), Si(110), and Si(111) disks were loaded perpendicular to their surface planes.

The CRM instrument, mapping, and fitting procedures were those used previously<sup>14</sup> with the following modification: An optically pumped semiconductor laser with a wavelength of 488 nm was used for excitation. The information depth for this wavelength was approximately 250 nm. The illumination power was set to 1 mW at the sample surface with the polarization axis aligned along the  $\langle 110 \rangle$  or  $\langle 112 \rangle$  directions for Si(001) or Si(111) and Si(110), respectively. An important exception to the prior study was made in the analysis of the hyperspectral CRM measurements: In addition to measuring the shift in the Raman peak of the longitudinal optical phonon in Si-I (from approximately  $520 \text{ cm}^{-1}$  at zero strain) to map residual strain exterior to the indentation impression, additional peaks were identified at smaller wave numbers to map residual phases within the indentation impression. In the Raman spectra, bands at (166, 184, **350**, 375, 397, 435, and 485)  $\text{cm}^{-1}$  have been assigned to Si-XII and bands occurring at (166, 384, 415, 433, and **465**)  $\text{cm}^{-1}$  have been assigned to Si-III as in previous studies.<sup>16,17</sup> The Raman spectrum of amorphous Si is characterized by four broadbands around 160, 300, 390, and **470**  $\text{cm}^{-1}$ .<sup>18,19</sup> Due to their large intensity in the

Raman spectra, the peaks with **bold** wave numbers were used as the primary peak for the fitting procedure, which employed a Pearson VII functional form and an iterative optimization. In generating the maps of the residual phases, regions of Si-III or Si-XII were mapped together, obviating to some degree the difficulty and uncertainty in assigning peaks to these two phases. For mapping the strain of the indentation zone, a shift in the Raman peak of the longitudinal optical phonon from its zero strain value to smaller frequencies is interpreted as tensile strain and to greater frequencies as compressive strain.<sup>20</sup>

### III. RESULTS

Figure 1 shows CRM phase maps of indentations on the three Si surface orientations: a large proportion of material in the circular contact impressions was transformed to a polycrystalline mixture of Si-III and Si-XII. However, the Si-I phase was also preserved in discrete ovoid areas within the impressions, although highly compressively strained compared to material external to the indentation (Fig. 2). Amorphous Si was accumulated in narrow zones between the Si-I and Si-III and Si-XII phases. For indentation loads greater than 80 mN (not shown here), transformed material Si-III and Si-XII extended over the entire contact impression, that is, no residual Si-I was observed within the contact impression. These map observations are consistent with previous nonmap studies of indentations formed using similar peak indentation strains: residual Si-I was detected within the contact impression by diffraction on impression cross sections<sup>21</sup> and by high-resolution transmission electron microscopy.<sup>22</sup>

The regions of preserved Si-I formed symmetrical patterns inside the contact impressions, dependent on the crystallographic orientation of the indented surface. For the (001) surface, a fourfold pattern was observed [Fig. 1(a)], with Si-I phase detected along the  $\pm[100]$  and  $\pm[010]$  directions, and a mix of Si-III and Si-XII phases located along the  $\pm[110]$  and  $\pm[1\bar{1}0]$  directions. For the (111) surface, Si-III and Si-XII phases extended along the  $[2\bar{1}\bar{1}]$ ,  $[\bar{1}2\bar{1}]$ , and  $[\bar{1}\bar{1}2]$  directions, whereas Si-I phase was concentrated along the opposite directions, generating a threefold symmetry [Fig. 1(b)]. The phase distribution map on the Si(110) surface had a twofold symmetry with preserved Si-I located along the  $\pm[\bar{1}10]$

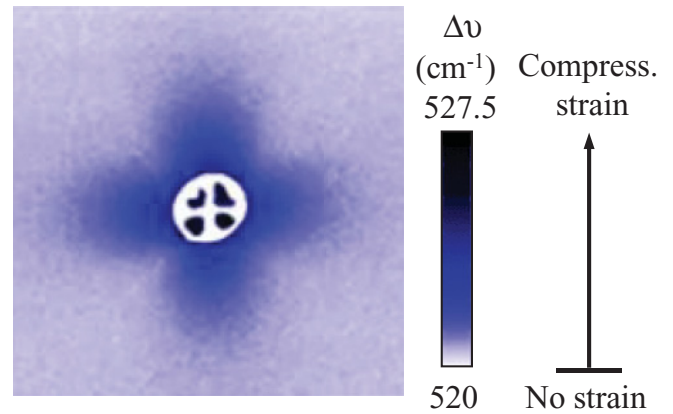


FIG. 2. (Color online) Map of the wave-number shift of the Si-I longitudinal optical phonon Raman peak in the indented region of a Si(100) disk. The shift to frequencies greater than 520  $\text{cm}^{-1}$  is interpreted as compressive strain. The white area inside the circular indentation impression indicates the presence of phases other than Si-I. Scan size is  $15 \times 15 \mu\text{m}$ .

directions and phase-transformed material along the  $\pm[001]$  directions [Fig. 1(c)].

### IV. DISCUSSION

When the shear strain induced by the indenter exceeds the critical threshold for slip in Si, dislocations initiate and propagate on active crystallographic slip planes and material is translated parallel to the slip planes causing distortion of the crystal structure in the slip directions.<sup>22,23</sup> Slip and dislocation activities beneath the indenter occur along converging slip planes,<sup>24</sup> and when the imposed shear is large enough, dislocations on intersecting slip planes entangle and combine to form sessile dislocations.<sup>25</sup> The entanglement hinders further dislocation motion and initiates phase transformation of material confined between the intersecting planes to accommodate further indentation deformation. The Si-I phase transforms to the Si-II structure on indentation loading as sublattices are compressed and shifted relatively to each other in opposite directions along slip planes.<sup>12,26</sup> Si-II transforms to a mix of polycrystalline phases rather than an amorphous state during unloading if the unloading strain rate is small,<sup>27</sup> as in the

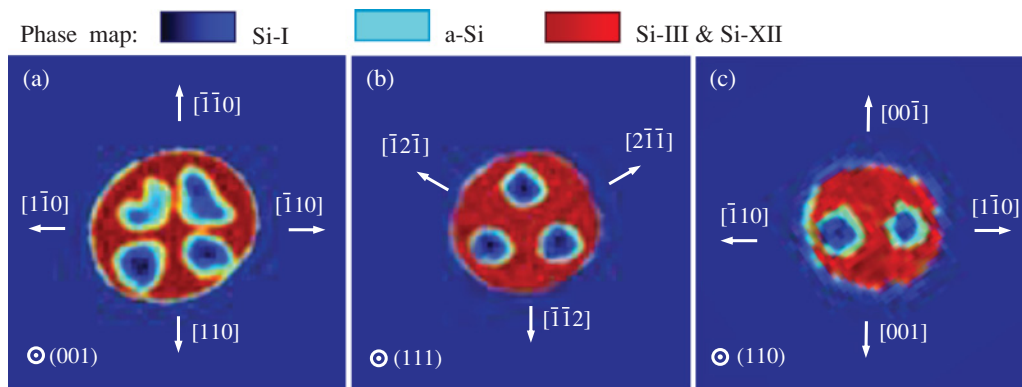


FIG. 1. (Color) Residual phase distribution maps for Si surfaces indented perpendicular to (a) (001), (b) (111), and (c) (110). Scan size is  $5 \times 5 \mu\text{m}$ .

present study: The tetrahedral bonding of the Si-II structure becomes inhomogeneously distorted along the silicon slip planes leading to the formation of Si-XII (rhombohedral) and subsequently, Si-III (body-centered cubic) phases.<sup>12,28</sup>

Due to the diamond-cubic structure of Si-I, material translation during slip takes place primarily on  $\{111\}$  slip systems, similar to face centered cubic crystals.<sup>23</sup> By calculating the Schmid factor,<sup>15</sup> a measure of the driving force for slip, it was determined that during indentation four slip planes were active for the (001) orientation, three for (111), and two for (110). Further, only two of the three possible slip systems were active on each of the unique slip planes (Fig. 3). For example,  $(11\bar{1})$  is common to all three orientations as an active slip system with two active dislocation Burgers vectors,  $\mathbf{b} = [10\bar{1}]$  and  $[01\bar{1}]$ , and a dislocation line direction of  $[\bar{1}\bar{1}0]$ . During indentation, deformation beneath the indenter is accommodated by motion of material by dislocation slip towards the indentation axis in directions perpendicular to the moving dislocation lines. When projected onto the indentation plane on which measurements were performed, for the example given, this is the  $[\bar{1}\bar{1}0]$  direction for the (001) indentation plane, the  $[11\bar{2}]$  direction for (111), and the  $[00\bar{1}]$  direction for (110) [Figs. 3(a)–3(c)]. This motion of material (and hydrostatic pressure) initiates phase transformation in these directions and the symmetric equivalents, in agreement with the observations of Figs. 1(a)–1(c):  $\pm[110]$  and  $\pm[\bar{1}\bar{1}0]$  for (001);  $[2\bar{1}\bar{1}]$ ,  $[\bar{1}2\bar{1}]$ , and  $[\bar{1}\bar{1}2]$  for (111); and  $\pm[001]$  for (110). The close proximity of the Si-I to phases with significantly different crystal structures led to the formation of transition zones containing material with an undefined, amorphous structure. The severe lattice distortion of the Si-I phase (as indicated by the large compressive strain) additionally promoted the amorphization of the intervening material.<sup>29</sup>

The observations made here—that the residual distributions of phases within contact impressions of indented Si are systematically inhomogeneous and anisotropic—are well explained by crystallographic slip considerations and are consistent with previous observations<sup>14,15</sup> that the residual stress fields exterior to contact impressions are also inhomogeneous and anisotropic. In the first case, slip on converging planes

eventually becomes locked, requiring phase transformation to accommodate further indentation deformation. In the second case, slip on diverging planes leads to imposed localized strains and a reaction residual stress field develops, although no doubt modified by the nature of the transformations within the contact impression. The slip considerations for both cases are similar, and hence it might have been expected that interior phase anisotropy should be observable if exterior stress field anisotropy was observed. What perhaps would not have been expected was that the interior effects would manifest as the inhomogeneous and anisotropic distribution of *untransformed* retained Si-I; an unusual observation that deserves some consideration.

Two factors are critical in determining the phases present in residual contact impressions in Si after complete indentation unloading: the peak indentation strain attained during loading and the unloading strain rate. The peak strain determines the extent of transformation from Si-I to Si-II. As slip-mediated plasticity is gradually impeded during loading by dislocation entanglement, the increased imposed indentation deformation is accommodated by the initiation and growth of domains of denser Si-II within the Si-I matrix. If the strain is great enough the domains extend to cover the entire contact impression surface. On unloading, the contact pressure is gradually relieved, and the Si-II phase becomes unstable and transforms to less dense crystalline phases, predominantly Si-III and Si-XII, or to an amorphous form, a-Si. The reverse transformation from Si-II to Si-I does not occur and residual Si-II does not occur. If the unloading strain rate is small enough, Si-II transforms to Si-III and Si-XII. If the unloading strain rate is great enough, Si-II transforms to a-Si; mixtures of residual Si-III, Si-XII, and a-Si within the contact impression occur for intermediate unloading strain rates.<sup>27,30,31</sup>

The characteristic indentation strain,  $\epsilon_I = 0.2(h_c/a)$ , where  $h_c$  is the indentation contact depth and  $a$  is the contact radius.<sup>32</sup> For a spherical indentation,  $(h_c/a) \approx (a/R)$ , where  $R$  is the indenter radius. For the conditions used in this paper on Si,  $a \approx 1.5 \mu\text{m}$  and  $R \approx 5 \mu\text{m}$  to give  $\epsilon_I \approx 0.060$ . For the conditions used in Bradby *et al.*<sup>30</sup> at a peak load of 80 mN on Si,  $a \approx 1.6 \mu\text{m}$  and  $R \approx 4.2 \mu\text{m}$  to give  $\epsilon_I \approx 0.075$ . For indentation loads greater than the 80 mN used here or in

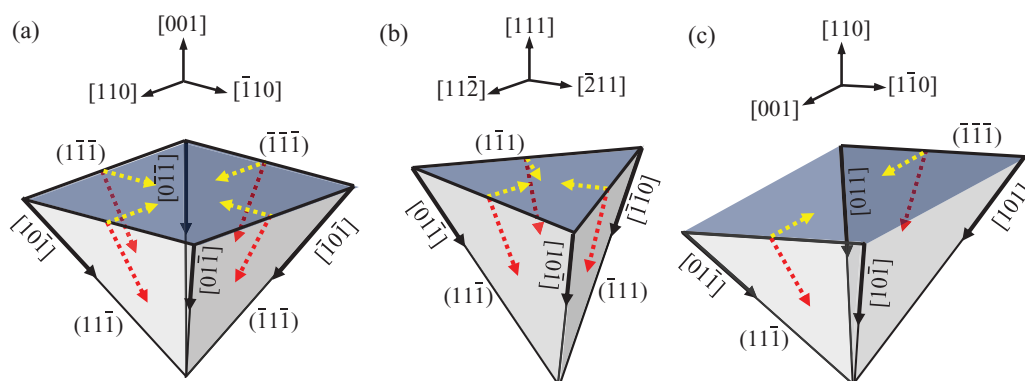


FIG. 3. (Color online) Schematic diagrams showing the four, three, and two slip planes (light gray) activated on indentation of Si perpendicular to surface planes (a) (001), (b) (111), or (c) (110), respectively. The black lines and arrows indicate the active dislocation line and Burgers vectors for the specific slip plane. The dark dashed arrows indicate the motion of material along the active slip plane, and the light dashed arrows are their projections onto the surface plane (dark grey).

Ref. 30 the contact radius is larger, and thus the indentation strain is greater. For pyramidal indentation,  $(h_c/a) \approx (1/\tan \phi)$ , where  $2\phi$  is the effective included angle of the indenter of the equivalent conical indenter. For a Vickers or Berkovich indenter,  $\phi \approx 70.3^\circ$ , and for a cube corner indenter,  $\phi \approx 42.3^\circ$ , to give  $\varepsilon_1 \approx 0.072$  for the Vickers or Berkovich and  $\varepsilon_1 \approx 0.22$  for the cube corner. Pyramidal indenters however, have sharp tips and edges, typically with radii from 50 nm to a few hundreds of nanometers. Hence, very small pyramidal indentations generate very large indentation strains at the tip and edges on initial contact; the global indentation strain decreases to the values given above for larger indentations for which the pyramidal geometry dominates, but the strains imposed locally at the tips and edges remain large. Hence, the greatest relative extent of formation of the Si-II phase on spherical indentation will occur at peak load, but for pyramidal indentation will be relatively invariant with load.

From the spherical indentation studies of Ref. 30 and others, and the results reported here,  $\varepsilon_1 \approx 0.025$  is not enough to initiate any irreversible deformation at indentations in Si, a strain of  $\varepsilon_1 \approx 0.04$  is enough to initiate slip and a small phase transformation zone, a strain of  $\varepsilon_1 \approx 0.060$  to  $\varepsilon_1 \approx 0.075$  is enough to develop the initiated transformation zone but still leave some untransformed material on the contact impression surface, and strains greater than  $\varepsilon_1 \approx 0.1$  lead to complete transformation of material on the contact impression surface. (The extent of transformation to Si-II at peak load is inferred from observations of Si-III, Si-XII, and a-Si at complete unload.) As complete transformation of material on the contact impression surface is always observed for Vickers and Berkovich indentation, the implication is that transformation of material during indentation is dominated by the initiation of transformation zones at the indenter tip and edges. Complete transformation is observed for cube corner indentation as well, but in that case the globally imposed indentation strain is probably great enough to completely transform material on the contact impression surface. The loading strain rate employed in Ref. 30 for a strain of  $\varepsilon_1 \approx 0.04$  was  $\dot{\varepsilon}_1 \approx 0.006 \text{ s}^{-1}$ , in this work for  $\varepsilon_1 \approx 0.06$  it was  $\dot{\varepsilon}_1 \approx 0.004 \text{ s}^{-1}$ , in Ref. 30 for  $\varepsilon_1 \approx 0.075$  it was  $\dot{\varepsilon}_1 \approx 0.003 \text{ s}^{-1}$ , and in the cube corner experiments of Pharr *et al.*<sup>5</sup> for  $\varepsilon_1 \approx 0.22$  it was  $\dot{\varepsilon}_1 \approx 0.003 \text{ s}^{-1}$ . The loading strain rates used in these studies were all comparable, but in the pyramidal indentation experiments of Jang *et al.*,<sup>27</sup> strains of  $\varepsilon_1 \approx 0.014$  to  $\varepsilon_1 \approx 0.22$  were used with a broader range of loading strain rates of  $\dot{\varepsilon}_1 \approx 0.001 \text{ s}^{-1}$  to  $\dot{\varepsilon}_1 \approx 0.014 \text{ s}^{-1}$  and the observed residual phases as a function of peak strain were similar to those noted above for the spherical indentations: no irreversible deformation for  $\varepsilon_1 \approx 0.01$ , small amounts of transformation at  $\varepsilon_1 \approx 0.04$ , and almost complete transformation for greater than  $\varepsilon_1 \approx 0.07$ . Taken together, these observations suggest the condition for islands of Si-I to be retained in the residual contact impression after indentation is  $0.04 < \varepsilon_1 < 0.1$ ; strains outside of this range either do not leave a residual contact impression or completely transform the contacted material to Si-II at peak load.

The transformation of Si-II to Si-III and Si-XII or to a-Si appears to be a function of strain rate. The retention of primarily crystalline phases within the contact impression here and in the experiments by Bradby *et al.* and Jang *et al.*

noted above appears to be related to the moderate unloading strain rates used. The early Vickers indentation measurement of Clarke *et al.*<sup>4</sup> used an unloading strain rate of  $\dot{\varepsilon}_1 \approx 3 \text{ s}^{-1}$ , resulting in complete amorphization of the residual contact impression, and in separate experiments to the same peak strains but using unloading strain rates up to  $\dot{\varepsilon}_1 \approx 0.085 \text{ s}^{-1}$ , Jang *et al.*<sup>27</sup> observed decreasing crystalline and increasing amorphous content in the contact impression.

In summary of these observations, a map has been compiled showing the residual Si phases in a contact impression as function of peak indentation strain and unloading indentation strain rate applied during the indentation (Fig. 4). The clear area for  $\varepsilon_1 < 0.04$  indicates that only Si-I remains after indentation, either because the indentation was completely elastic or because the peak indentation strain was not great enough to trigger a transformation. The single hatched area for  $0.04 < \varepsilon_1 < 0.1$  indicates that some Si-I remains after indentation, with the amount retained decreasing as the strain increases from 0.04 to 0.1. The location of the experiments in the current work is indicated in this region by the symbol. The double hatched area for  $\varepsilon_1 > 0.1$  indicates that no Si-I remains after indentation and that, depending on the unloading strain rate, the material is completely transformed to either Si-III and Si-XII or a-Si. It should be noted that this map is assembled from data gathered mostly on Si(001) samples. The peak strain boundaries for partial and complete phase transformation proposed here will likely differ for other crystallographic orientations, as the threshold pressure (and strain) for initiating phase transformation processes is highly dependent on the crystallographic orientation of the Si sample.<sup>14,33</sup>

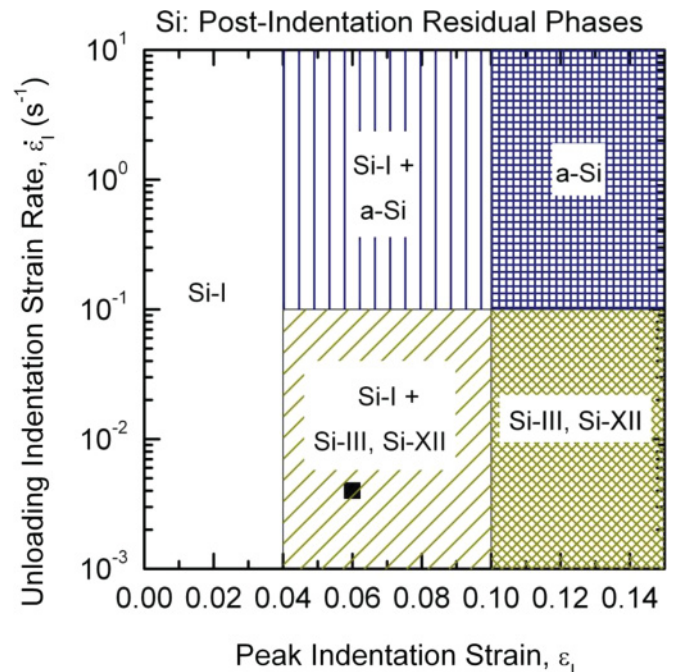


FIG. 4. (Color online) Map of the phases retained in Si post-indentation as a function of peak indentation strain and unloading indentation strain rate. The symbol indicates the location of the experiments conducted in this study.

## V. CONCLUSIONS

The anisotropic nature of indentation phase transformation in Si was observed directly in experiments confirming predictions from theoretical studies.<sup>11–13</sup> The Si-I phase was locally preserved and an anisotropic pattern in the distribution of the transformed phases Si-XII and Si-III was revealed. The anisotropy of the phase transformation is linked to the  $\{111\}\langle 110 \rangle$  slip systems of the Si-I phase activated during indentation. The pattern symmetry is dependent on the orientation and number of the slip systems activated for the indented surface in accordance with the Schmid rule.

Converting test-specific parameters (e.g., maximum indentation load, unloading rate) into universal parameters of peak indentation strain and unloading strain rate enabled direct comparison of the above observations of post-indentation Si phases with those observed in other studies. This comparison revealed a dependence of the presence of specific post-indentation Si phases with the peak indentation strain and

unloading strain rate, as depicted in the map in Fig. 4. The map indicates that key to the *observation* of anisotropic phase transformation is the peak indentation strain; the value has to be great enough to initiate the phase transformation but still small enough to hinder expansion of the transformation over the entire contact region. Another implication of this map is that large unloading strain rates (e.g., by use of fast unloading rates) would result in anisotropic phase transformation, but with a-Si surrounding preserved Si-I islands for the appropriate range of indentation strain.

Although this study reports on the residual distribution of Si-III and Si-XII phases, it can be inferred that Si-II induced during loading is distributed in a similar anisotropic manner, as the phase transformation is irreversible at room temperature. It is interesting to speculate on the possible role that anisotropic transformation to the metallic Si-II phase and, thus, anisotropic change in conductivity and ductility may play in the operation of microelectromechanical system and nanoelectromechanical system devices.

\*robert.cook@nist.gov

<sup>1</sup>J. Yan, H. Zhao, and T. Kuriyagawa, *Semicond. Sci. Technol.* **24**, 075018 (2009).

<sup>2</sup>Y. Wang, J. Zhang, J. Wu, J. L. Coffey, Z. Lin, S. V. Sinogeikin, W. Yang, and Y. Zhao, *Nano Lett.* **8**, 2891 (2008).

<sup>3</sup>P. Valentini, W. W. Gerberich, and T. Dumitrică, *Phys. Rev. Lett.* **99**, 175701 (2007).

<sup>4</sup>D. R. Clarke, M. C. Kroll, P. D. Kirchner, R. F. Cook, and B. J. Hockey, *Phys. Rev. Lett.* **60**, 2156 (1988).

<sup>5</sup>G. M. Pharr, W. C. Oliver, and D. S. Harding, *J. Mater. Res.* **6**, 1129 (1991).

<sup>6</sup>K. Gaál-Nagy and D. Strauch, *Phys. Rev. B* **73**, 134101 (2006).

<sup>7</sup>H. Saka, A. Shimatani, M. Sukanuma, and Suprijadi, *Philos. Mag. A* **82**, 1971 (2002).

<sup>8</sup>I. Zarudi, L. C. Zhang, J. Zou, and T. Vodenitcharova, *J. Mater. Res.* **19**, 3320 (2004).

<sup>9</sup>L. J. Vandeperre, F. Guiliani, S. J. Lloyd, and W. J. Clegg, *Acta Mater.* **55**, 6307 (2007).

<sup>10</sup>T. Vodenitcharova and L.C. Zhang, *Int. J. Solids Struct.* **40**, 2989 (2003).

<sup>11</sup>G. S. Smith, E. B. Tadmor, N. Bernstein, and E. Kaxiras, *Acta Mater.* **49**, 4089 (2001).

<sup>12</sup>D. E. Kim and S. I. Oh, *Nanotechnology* **17**, 2259 (2006).

<sup>13</sup>Y. H. Lin, T.-C. Chen, P.-F. Yang, S.-R. Jian, and Y.-S. Lai, *Appl. Surf. Sci.* **254**, 1415 (2007).

<sup>14</sup>Y. B. Gerbig, S. J. Stranick, D. J. Morris, M. D. Vaudin, and R. F. Cook, *J. Mater. Res.* **24**, 1172 (2009).

<sup>15</sup>Y. B. Gerbig, S. J. Stranick, and R. F. Cook, *Scr. Mater.* **63**, 512 (2010).

<sup>16</sup>R. J. Koblinska, S. A. Solin, M. Selders, R. K. Chang, R. Alben, M. F. Thorpe, and D. Weaire, *Phys. Rev. Lett.* **29**, 725 (1972).

<sup>17</sup>D. Ge, V. Domnich, and Y. Gogotsi, *J. Appl. Phys.* **93**, 2423 (2003).

<sup>18</sup>J. E. Smith Jr., M. H. Brodsky, B. L. Crowder, M. L. Nathan, and A. Pinczuk, *Phys. Rev. Lett.* **26**, 642 (1971).

<sup>19</sup>N. Maley, D. Beeman, and J. S. Lannin, *Phys. Rev. B* **38**, 10611 (1988).

<sup>20</sup>V. Senez, A. Armigliato, I. De Wolf, G. Carnevale, R. Balboni, S. Frabboni, and A. Benedetti, *J. Appl. Phys.* **94**, 5574 (2003).

<sup>21</sup>J. E. Bradby, J. S. Williams, J. Wong-Leung, M. V. Swain, and P. Munroe, *Mater. Res. Soc. Symp.* **649**, Q8.10.1 (2001).

<sup>22</sup>I. Zarudi, J. Zou, and L. C. Zhang, *Appl. Phys. Lett.* **82**, 874 (2003).

<sup>23</sup>L. B. Hansen, K. Stokbro, B. I. Lundqvist, K. W. Jacobsen, and D. M. Deaven, *Phys. Rev. Lett.* **75**, 4444 (1995).

<sup>24</sup>S. G. Roberts, P. D. Warren, and P. B. Hirsch, *J. Mater. Res.* **1**, 186 (1986).

<sup>25</sup>K. J. Van Vliet, J. Li, T. Zhu, S. Yip, and S. Suresh, *Phys. Rev. B* **67**, 104105 (2003).

<sup>26</sup>S. M.-M. Dubois, G.-M. Rignanese, T. Pardoen, and J.-C. Charlier, *Phys. Rev. B* **74**, 235203 (2006).

<sup>27</sup>J. Jang, M. J. Lance, S. Wen, T. Y. Tsui, and G. M. Pharr, *Acta Mater.* **53**, 1759 (2005).

<sup>28</sup>J. Crain, G. J. Ackland, J. R. Maclean, R. O. Piltz, P. D. Hatton, and G. S. Pawley, *Phys. Rev. B* **50**, 13043 (1994).

<sup>29</sup>Y. Q. Wu, X. Y. Yang, and Y. B. Xu, *Acta Mater.* **47**, 2431 (1999).

<sup>30</sup>J. E. Bradby, J. S. Williams, J. Wong-Leung, M. V. Swain, and P. Munroe, *J. Mater. Res.* **16**, 1500 (2001).

<sup>31</sup>A. Kailer, Y. G. Gogotsi, and K. G. Nickel, *J. Appl. Phys.* **81**, 3057 (1997).

<sup>32</sup>D. Tabor, *The Hardness of Metals* (Clarendon Press, Oxford, United Kingdom, 1951).

<sup>33</sup>M. C. Gupta and A. L. Ruoff, *J. Appl. Phys.* **51**, 1072 (1980).